

University of Groningen

A structural view onto disease-linked mutations in the human neutral amino acid exchanger ASCT1

Stehantsev, Pavlo; Stetsenko, Artem; Nemchinova, Mariia; Aduri, Nanda Gowtham; Marrink, Siewert; Gati, Cornelius; Guskov, Albert

Published in:
Computational and Structural Biotechnology Journal

DOI:
[10.1016/j.csbj.2021.09.015](https://doi.org/10.1016/j.csbj.2021.09.015)

IMPORTANT NOTE: You are advised to consult the publisher's version (publisher's PDF) if you wish to cite from it. Please check the document version below.

Document Version
Version created as part of publication process; publisher's layout; not normally made publicly available

Publication date:
2021

[Link to publication in University of Groningen/UMCG research database](#)

Citation for published version (APA):

Stehantsev, P., Stetsenko, A., Nemchinova, M., Aduri, N. G., Marrink, S., Gati, C., & Guskov, A. (2021). A structural view onto disease-linked mutations in the human neutral amino acid exchanger ASCT1. *Computational and Structural Biotechnology Journal*, 19, 5246-5254. <https://doi.org/10.1016/j.csbj.2021.09.015>

Copyright

Other than for strictly personal use, it is not permitted to download or to forward/distribute the text or part of it without the consent of the author(s) and/or copyright holder(s), unless the work is under an open content license (like Creative Commons).

The publication may also be distributed here under the terms of Article 25fa of the Dutch Copyright Act, indicated by the "Taverne" license. More information can be found on the University of Groningen website: <https://www.rug.nl/library/open-access/self-archiving-pure/taverne-amendment>.

Take-down policy

If you believe that this document breaches copyright please contact us providing details, and we will remove access to the work immediately and investigate your claim.

Downloaded from the University of Groningen/UMCG research database (Pure): <http://www.rug.nl/research/portal>. For technical reasons the number of authors shown on this cover page is limited to 10 maximum.

Journal Pre-proofs

A structural view onto disease-linked mutations in the human neutral amino acid exchanger ASCT1

Pavlo Stehantsev, Artem Stetsenko, Mariia Nemchinova, Nanda Gowtham Aduri, Siewert J. Marrink, Cornelius Gati, Albert Guskov

PII: S2001-0370(21)00400-1
DOI: <https://doi.org/10.1016/j.csbj.2021.09.015>
Reference: CSBJ 1216

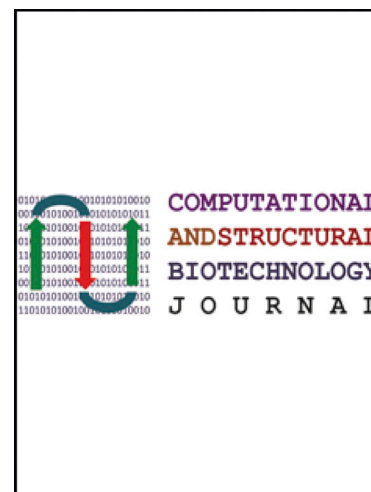
To appear in: *Computational and Structural Biotechnology Journal*

Received Date: 30 July 2021
Revised Date: 14 September 2021
Accepted Date: 14 September 2021

Please cite this article as: P. Stehantsev, A. Stetsenko, M. Nemchinova, N. Gowtham Aduri, S.J. Marrink, C. Gati, A. Guskov, A structural view onto disease-linked mutations in the human neutral amino acid exchanger ASCT1, *Computational and Structural Biotechnology Journal* (2021), doi: <https://doi.org/10.1016/j.csbj.2021.09.015>

This is a PDF file of an article that has undergone enhancements after acceptance, such as the addition of a cover page and metadata, and formatting for readability, but it is not yet the definitive version of record. This version will undergo additional copyediting, typesetting and review before it is published in its final form, but we are providing this version to give early visibility of the article. Please note that, during the production process, errors may be discovered which could affect the content, and all legal disclaimers that apply to the journal pertain.

© 2021 The Author(s). Published by Elsevier B.V. on behalf of Research Network of Computational and Structural Biotechnology.



A structural view onto disease-linked mutations in the human neutral amino acid exchanger ASCT1

Pavlo Stehantsev¹†, Artem Stetsenko¹†, Mariia Nemchinova¹, Nanda Gowtham Aduri², Siewert J. Marrink¹, Cornelius Gati² and Albert Guskov^{1,3*}.

¹Groningen Biomolecular Sciences and Biotechnology Institute, University of Groningen, The Netherlands

²Department of Biological Sciences, Bridge Institute, USC Michelson Center for Convergent Bioscience, University of Southern California, Los Angeles, CA, USA

³Moscow Institute of Physics and Technology, Dolgoprudny, Russia

†These authors contributed equally to this work

* Correspondence to: a.guskov@rug.nl

Abstract

The ASCT1 transporter of the SLC1 family is largely involved in equilibration of neutral amino acids' pools across the plasma membrane and plays a prominent role in the transport of both L- and D-isomers of serine, essential for the normal functioning of the central nervous system in mammals. A number of mutations in ASCT1 (E256K, G381R, R457W) have been linked to severe neurodevelopmental disorders, however in the absence of ASCT1 structure it is hard to understand their impact on substrate transport. To ameliorate that we have determined a cryo-EM structure of human ASCT1 at 4.2 Å resolution and performed functional transport assays and molecular dynamics simulations, which revealed that given mutations lead to the diminished transport capability of ASCT1 caused by instability of transporter and impeded transport cycle.

1. Introduction

Alanine Serine Cysteine Transporter 1 (ASCT1) belongs to the solute carrier 1 family (SLC1) of proteins, which includes the subfamily of Excitatory Amino Acid Transporters (EAAT1-5) and another neutral amino acid exchanger, ASCT2 [1]–[3]. EAATs use the sodium gradient as an energy source to re-uptake the neurotransmitter glutamate (as well as L- or D-aspartate) in the synaptic cleft to prevent the overstimulation of glutamate receptors and avoid excitotoxicity [4]–[6]. The transport is also coupled to H⁺ and counter-transport of K⁺ ion [7]–[9], and additionally all transporters reveal different levels of uncoupled chloride conductance [10]–[13].

ASCT proteins, in contrast, do not concentrate their substrates, but perform the obligatory exchange of the amino acid pools, although the transport is still coupled to Na⁺ [14]–[16]. There is still no consensus whether the transport is electroneutral (this work and [14], [15]) or electrogenic (discussed in [17]). ASCTs are ubiquitously expressed with the highest expression of ASCT2 in placenta, lung, skeletal muscle, kidney, pancreas, and intestine and of

44 ASCT1 in brain, muscle, and pancreas [18]–[21]. ASCT2 has gained a lot of focus since it has
45 been linked to numerous cancers (see recent reviews [22], [23]) where it is involved into the
46 transport of glutamine, which is essential for carcinogenesis as it can be used to fuel the TCA
47 cycle [24]. Up to date ASCT1 was associated only with esophageal adenocarcinomas [25] and
48 prostate cancer [26], albeit it was shown that ASCT1 is not capable to transport glutamine [27].

49 L-Ser is a non-essential amino acid, however there is an active de novo synthesis of L-
50 Ser in the brain [28] as it is a critical precursor for the synthesis of L-Cys, phosphatidyl-L-Ser,
51 sphingolipids, and most importantly of D-Ser [29], [30]. D-Ser is a major co-agonist of N-
52 methyl-D-aspartate receptors [31], [32] produced by racemization of L-Ser by the specific
53 enzyme serine racemase [33], which is heavily expressed in neurons, and to some extent in
54 glial cells [34]–[36]. However the synthesis of L-Ser is confined to astrocytes [37], hence it
55 must be somehow shuttled to serine racemase (so-called serine shuttle [38]), and the major role
56 in L-Ser transport is ascribed to ASCT1 [39], which is capable to exchange L-Ser for D-Ser or
57 any other suitable substrate. Interestingly, both ASCT1 and ASCT2 were shown to transport
58 L-Ser and D-Ser in transfected HEK293 cells [40], [41], hence perhaps there is an interplay
59 between two transporters with the preferential expression of ASCT1 in astrocytes [18], [39]
60 and ASCT2 in neurons [42].

61 Experiments on ASCT1-knock out mice revealed numerous motor and
62 neurodevelopmental disorders [39] similar to those linked to nonsense and missense mutations
63 in ASCT1 in humans (recently reviewed in [43]), which cause autosomal recessive
64 neurodevelopmental disorders, generally termed as spastic tetraplegia, thin corpus callosum,
65 and progressive microcephaly (SPATCCM, Online Mendelian Inheritance in Man # 616657).
66 Up to date characterized nonsense mutations are Y191* (so only a partial scaffold domain and
67 almost none of a transport domain produced), which leads to microcephaly, tonic-clonic
68 seizures, motor and speech delays [44]; W453* (almost complete protein produced, except
69 TM8 and C-terminus), leading to microcephaly, motor and dyscognitive seizures, speech delay
70 [45]; one frame shift mutation L315*fs (hence the transport domain does not follow the
71 canonical sequence), causing microcephaly, infantile spasms, speech delay [46]; and three
72 missense mutations – E256K, G381R, R457W, leading to various degrees of similar disorders
73 and disabilities [46]–[49].

74 To be able to map these mutations and get a better understanding how they lead to the
75 malfunctioning of this transporter, we solved the ASCT1 structure using single-particle cryo-
76 EM technique to the overall resolution of 4.2 Å and performed subsequent all-atom molecular

77 dynamics (MD) simulations on the aforementioned missense mutations as well as their
78 functional characterization.

79 2. Materials and Methods

80 2.1. Transformation and cloning

81 The pPICZ-B vector with incorporated human wild-type ASCT1 gene was ordered from
82 GenScript. Mutants E256K (forward primer 5' CAATCCCTCAACAAGGCGACGATGGTGCTGG
83 3'; reverse primer 5' CCAGCACCATCGTCGCCTTGTGAGGGAATTG 3') and R457W (forward
84 primer 5' TGGATTGTGGACTGGACCACCACGGTGGTGAA 3', reverse primer 5'
85 TTCACCACCGTGGTGGTCCAGTCCACAATCCA 3') were introduced using QuickChange site-
86 directed mutagenesis on the ordered pPICZ-B vector with the inserted human wild-type ASCT1 gene.
87 The constructs were transformed into chemically competent *Escherichia coli* DH5 α cells to
88 produce ~10 μ g of the plasmid. The isolated plasmids were linearised with *PmeI*, transformed
89 into sorbitol-treated *P. pastoris* strain X-33 by electroporation, and grown on the Yeast Extract
90 Peptone Dextrose (YPDS) medium agar plates at 30 °C for four days. Zeocin (Invitrogen) with
91 100 μ g/mL, 500 μ g/mL and 1000 μ g/mL concentrations was used as a selection marker. For
92 analysis, a few colonies from each plate were picked and grown in 5 mL Yeast Extract Peptone
93 Dextrose (YPD) medium with 100 μ g/mL Zeocin (Invitrogen) in CELLSTAR® CELLreactor
94 tubes at 30 °C, 200 rpm, overnight.

95

96 2.2. Protein expression and purification

97 For large-scale protein production, the transformed cells were pre-cultured in 11 baffled flask
98 with 100 mL of the Buffered Glycerol-complex (BMGY) medium without antibiotics at 30 °C,
99 200 rpm, overnight. The next day, the medium was replaced with the Buffered Methanol-
100 complex (BMMY) setting up the start OD₆₀₀ to 1.0 in 500 ml. The cells were expressed for 72
101 h in a 5l baffled flask at 30 °C, 200 rpm, with addition of 0.5% methanol for every 24 hours
102 period.

103 Further, the cells were isolated by centrifugation (4,500 g, 10 min, 4 °C), resuspended
104 in Buffer A (50 mM Tris-HCl, pH 7.4, 250 mM NaCl, 5% (vol/vol) glycerol), flash frozen in
105 liquid nitrogen and stored at -80 °C. The cells were broken with Maximator High Pressure
106 Homogenizer Type HPL6 (Maximator GmbH). The cells were supplied with 0.1 mg ml⁻¹
107 DNase (Sigma-Aldrich) and 3 mM MgSO₄, and broken in three passages (39 kPsi, 4 °C). After
108 the second passage, the broken cells were supplied with 1 mM phenylmethylsulfonyl fluoride
109 (Roche) protease inhibitor. The cell lysate was centrifuged (10,000 g, 30 min, 4 °C) to remove

110 cell debris, and the supernatant was ultracentrifuged (194,000 g, 120 min, 4 °C) to sediment
111 membrane fractions. The membrane fractions were resuspended in Buffer B (50 mM Tris-HCl,
112 pH 7.4, 250 mM NaCl, 5% (vol/vol) glycerol), flash frozen and stored at -80 °C in aliquots of
113 membrane vesicles from ~ 2.5 g cells.

114 To purify the wild-type or mutant proteins, an aliquot of the membrane vesicles was
115 kept with Buffer C (50 mM Tris-HCl, pH 7.4, 250 mM NaCl, 5% (vol/vol) glycerol, 1 mM L-
116 serine (ACROS Organics), 1% DDM and 0.1% CHS (Anatrace)) and stirring for 1 h at 4 °C.
117 The sample was ultracentrifuged (236,000 g, 30 min, 4 °C) to remove unsolubilized particles.
118 The supernatant was incubated for 1 h at 4 °C while gently rocking with Ni²⁺-sepharose resin,
119 column volume of 0.5 ml, which had been equilibrated with 10 times CV of Buffer D (50 mM
120 Tris-HCl, pH 7.4, 250 mM NaCl, 40 mM Imidazole, 5% (vol/vol) glycerol, 1 mM L-serine
121 (ACROS Organics), 0.02% DDM and 0.002% CHS (Anatrace)). Subsequently, the suspension
122 was poured into a 10-ml disposable column (Bio-Rad). The unbound material was let to flow
123 through, the column was washed with the Buffer D, and ASCT1 was eluted with Buffer E (50
124 mM Tris-HCl, pH 7.4, 250 mM NaCl, 500 mM Imidazole, 5% (vol/vol) glycerol, 1 mM L-
125 serine (ACROS Organics), 0.02% DDM and 0.002% CHS (Anatrace)). Elution fraction was
126 applied to size-exclusion chromatography column Superdex 200 10/300 (GE-Healthcare) that
127 preliminarily was equilibrated with Buffer F (50 mM Tris-HCl, pH 7.4, 250 mM NaCl, 5%
128 (vol/vol) glycerol, 1 mM L-serine (ACROS Organics), 0.02% DDM and 0.002% CHS
129 (Anatrace)). Protein-containing fractions were used for reconstitution into proteoliposomes or
130 concentrated with Vivaspin Turbo 4 (Sartorius) concentrator with 100 kDa cutoff size for the
131 following preparation for Cryo-EM data collection.

132

133 2.3. *Reconstitution into proteoliposomes*

134 To reconstitute the proteins into liposomes, we used a mixture of *Escherichia coli* lipids and
135 phosphatidylcholine in a ratio of 3:1 that additionally contains 5% (wt/wt) or 10% (wt/wt)
136 cholesterol (Avanti Polar lipids) in indicated experiments. An aliquot of the liposome mixture
137 was thawed and extruded through a 400-nm-diameter polycarbonate filter (Avestin) and
138 afterward diluted with Buffer G (20 mM Tris-HCl, pH 7.0) to the final concentration of 4 mg
139 ml⁻¹. Further, the mixture was destabilized with 10% Triton X-100 and fused with freshly
140 purified wild-type or mutant ASCT1 in a ratio of 1:250 (protein/lipids). The mixture was
141 nutated for 30 minutes at room temperature. Afterward, to remove detergent we added Bio-
142 beads in four steps: first, add 25 mg ml⁻¹ for 30 min at room temperature; second, add 15 mg
143 ml⁻¹ for 1 h at 4 °C; third, add 19 mg ml⁻¹ with an overnight incubation at 4 °C; and lastly add

144 29 mg ml⁻¹ for 2 h at 4 °C on the next morning. Proteoliposomes were isolated from the Bio-
145 beads, collected by ultracentrifugation (443,000 g, 25 min, 4 °C), and resuspended into Buffer
146 G to final concentration 20 mg ml⁻¹, aliquoted, flash frozen, and stored in liquid nitrogen.

147

148 2.4. Radiolabeled transport assays

149 For transport assays, an aliquot of proteoliposomes was thawed at room temperature with the
150 following addition of 10 mM unlabeled L-serine or indicated L-amino acid and 50 mM NaCl.
151 The resuspension was exposed to three cycles of freeze-thaw and extruded with 11 passages
152 through 400-nm-diameter polycarbonate filter (Avestin). The proteoliposomes were
153 resuspended with Buffer G and ultracentrifuged (443,000 g, 25 min, 4 °C) to remove excess of
154 the substrate and again resuspended in the Buffer G with final concentration 20 mg ml⁻¹ that
155 contains 10 µg of the protein in total. The assays were performed at a water bath with set 25 °C
156 and stirring 200 rpm. The external buffer contains 50 mM NaCl, 50 µM non-radioactive amino
157 acid of interest, 0.3 µM [¹⁴C]L-amino acid (PerkinElmer), and 20 mM Tris-HCl, pH 7.0 in the
158 total volume of 600 µL. As a start point, 80 µL of the external buffer was quenched (to stop
159 transport) by 2 mL of cold Buffer G, and the proteoliposomes with 1.6 µg of protein were
160 added and immediately filtered through 0.45 nm pore-size filter (Protran BA-85, Whatman)
161 and the filter stored. To start the transport, the rest of the proteoliposomes that contain 8.4 µg
162 of the protein were diluted in 520 µL of the external buffer. For each time point, 80 µL of the
163 external buffer was quenched by 2 mL of cold Buffer G, filtered through 0.45 nm pore-size
164 filter (Protran BA-85, Whatman), washed by another 2 mL of cold Buffer G and stored. After
165 the last time point, three fresh filters were treated by 20 µL of the external buffer and stored for
166 calculations of the total counts. After the experiment, the filters were dissolved in 2 mL filter
167 count scintillation liquid (Emulsifier Scintillator Plus, PerkinElmer). The radioactivity of the
168 filters was measured with a PerkinElmer Tri-Carb 2800 RT scintillation counter. Error bars are
169 represented at least three independent experiments.

170 For experiments to test the electrogenic nature of the exchange, the proteoliposomes
171 were loaded with 10 mM unlabeled L-serine (ACROS Organics) and 50 mM KCl or 50 mM
172 NaCl for a negative control. During the experiment, the external buffer was additionally
173 supplied with 3 µM valinomycin at indicated time points. The assays were performed as
174 described above.

175 For the competition transport assays the proteoliposomes were loaded with 10 mM
176 unlabeled L-serine (ACROS Organics) and 50 mM NaCl. The external buffer for the assays
177 was additionally supplied with 1 mM of the indicated unlabeled amino acid, 50 mM NaCl, 0.3

178 μM [^{14}C]L-serine (PerkinElmer), and 20 mM Tris-HCl, pH 7.0. After 30 minutes of the
179 exchange the aliquots of data points were collected identically to the competition transport
180 assays.

181 For the exchange transport assays the proteoliposomes were loaded with 10 mM
182 unlabeled indicated amino acid and 50 mM NaCl. The external buffer contains 50 mM NaCl,
183 50 μM non-radioactive L-serine, 0.3 μM [^{14}C]L-serine (PerkinElmer), and 20 mM Tris-HCl,
184 pH 7.0 After 30 minutes of the exchange the aliquots of data points were collected identically
185 to the competition transport assays.

186

187 2.5. *Cryo-EM sample preparation, imaging and data processing*

188 For cryo-EM sample preparation, 3 μl of concentrated sample at ~ 8 mg/ml (100 kDa cut-off,
189 Amicon), was applied to freshly glow-discharged (easiGlo Ted Pella, 20 mA, 40 s) grids
190 (Quantifoil Au 1.2/1.3 200 mesh), blotted and plunge frozen in liquid ethane using a Leica GP2
191 plunger. Data collection was carried on a Titan Krios (Thermo Fisher Scientific) equipped with
192 a K3 direct-electron detector (Gatan). SerialEM [50] was used for automated data collection,
193 using an image-shift based (9 holes) procedure, with a defocus range of -1.0 to -2.0 μm and a
194 dose rate of 15 $\text{e}^-/\text{px}/\text{s}$ and a pixel size of 0.8521 \AA . Micrographs were collected with 50 ms
195 exposure per frame for a total of 3 seconds, resulting in 60 frames total. Data processing was
196 carried out using established protocols, as part of the software packages RELION [51] (version
197 3.1.2) and cryoSPARC (v3.2.0). A total of 4899 micrographs were subjected to motion
198 correction (MotionCor2 [52]) and CTF estimation using CTFFIND4 [53], followed by
199 reference-free and reference-based particle picking, 2D classification and final reconstruction
200 in cryoSPARC using non-uniform refinement [54], while applying C3 symmetry, resulting in
201 a map of 4.2 \AA resolution (FSC=0.143). All attempts to reconstruct in C1 resulted in maps of
202 lower resolution (~ 6 \AA), while not showing any asymmetric features.

203

204 2.6. *Model building and refinement*

205 As a starting model we used ASCT2 structure (PDB ID 6GCT), which was manually adjusted
206 in Coot to match the sequence of ASCT1 and fit the density. Real space refinement and
207 validation was done in Phenix.

208

209 2.7. *Molecular dynamics simulations*

210 We performed atomistic MD simulations of the obtained cryo-EM structure of ASCT1 wild-
211 type (WT) and in-silico designed mutants (E256K, G381R, R457W) embedded in a lipid
212 membrane in aqueous salt solutions. All MD simulations were performed using the MD
213 package Gromacs (version 2018.1) [55] and the CHARMM36 force field [56]–[58]. The
214 membrane builder tool of the CHARMM-GUI [59], [60] ([http://www.charmm-
215 gui.org/?doc=input/membrane.bilayer](http://www.charmm-gui.org/?doc=input/membrane.bilayer)) was used to embed the protein structure in a rectangular
216 lipid bilayer composed of a mixture of 400 molecules of 1-palmitoyl-2-oleoyl-sn-glycero-3-
217 phosphoethanolamine (POPE), 1-palmitoyl-2-oleoyl-sn-glycero-3-phosphoglycerol (POPG)
218 and 1-palmitoyl-2-oleoyl-sn-glycero-3-phosphocholine (POPC) lipids in the ratio 3:3:2 as was
219 used in the proteoliposomes in our *in-vitro* experiments and solvated with 150 mM aqueous
220 NaCl solution. The box dimensions of the system are $130 \times 130 \times 130$ Å. The system was then
221 solvated with TIP3P water molecules [61] such that every protein atom was at least 12 Å away
222 from the side of the box. Periodic boundary conditions were employed and the particle-mesh
223 Ewald method [62], [63] was used for treatment of long-range electrostatic interactions. The
224 systems were optimized and equilibrated for 1 ns in the NVT ensemble and 20 ns in the NPT
225 ensemble. After the equilibration stages, a 1 μ s long unrestrained run was carried out for each
226 system. The pressure was maintained at 1 atm semi-isotropically with the Parinello–Rahman
227 barostat [64], [65] and a coupling constant of 1.0 ps. The simulations were conducted at a
228 constant temperature of 303.15 K using the Nosé-Hoover thermostat [66], [67]. The total
229 number of atoms in the simulation box was $\sim 230\,000$ atoms. Visual inspection of the
230 trajectories was performed with VMD [68] and the open source version of PyMOL.

231
232

233 3. Results

234 3.1. Functional characterization

235 We expressed unmodified human ASCT1 (SLC1A4) as well as two mutant forms (E256K and
236 R457W) in the yeast *Pichia pastoris*, and purified it by combination of immobilized metal
237 affinity and size exclusion chromatography (Supplementary Fig. 1). To test that the WT protein
238 is functional, we reconstituted the protein into proteoliposomes (according to the published
239 protocol [69]) and performed transport assays. Reconstituted ASCT1 readily transports
240 radioactive L-Ser and L-Ala but it does not transport L-Gln (Figure 1a, c, e). Interestingly, the
241 uptake of L-Ser is inversely correlated to the cholesterol content in the proteoliposomes – the
242 increase of cholesterol from 0 to 10% leads to more than 2-fold decrease in the substrate uptake
243 (Fig. 1a). Similarly to ASCT2 [14], using our experimental setup, the exchange of amino acid

244 pools via ASCT1 **seems to be** electroneutral as an addition of valinomycin showed no effect
245 on the transport (Fig. 1b).

246 Furthermore, we tested substrate specificity of ASCT1 with the following setups: (i) we
247 monitored the uptake of radioactive L-Ser into the proteoliposomes in the 1 mM excess of an
248 amino acid in the outside buffer ('inward competition'); and (ii) with the 10 mM excess of an
249 amino acid inside proteoliposomes ('outward competition'). We observed **the significant**
250 **decrease in the uptake of radioactive L-Ser in the presence of** L-Ala, L-Cys, L-Thr and L-Asn,
251 **and the moderate decrease in the presence of** D-Ser and L-Pro (Fig. 1c). The presence of L-
252 Met, L-Val, L-Asp, L-Gln, L-Trp, L-Lys and Gly did not affect the uptake of radioactive L-
253 Ser. In the setup (ii), we observed **the uptake of the radioactive L-Ser into proteoliposomes,**
254 **indicating that indeed** an exchange of L-Asn, L-Pro, and D-Ser trapped inside the
255 proteoliposomes with the external substrate **has taken place** (Fig. 1d), **but we observed no**
256 **exchange of internal unlabeled L-Gln with external [³H]L-Gln (Fig. 1e).** **The introduced point**
257 **mutations were detrimental for the substrate uptake (Fig. 1f and §3.3).**

258

259 3.2. Structure of ASCT1

260 We solved the structure of human ASCT1 incorporated into the n-dodecyl- β -D-
261 maltopyranoside (DDM) micelles using single particle cryo-EM technique at the overall
262 resolution of 4.2 Å (Table 1, Supplementary Fig. 2). ASCT1 shares over 56% sequence identity
263 with ASCT2 and as all other members of SLC1 family characterized up to date [14], [70]–[72]
264 it forms a homotrimer (Fig. 2a), with the core scaffold domain (TMS 1, 2, 4, and 5) and three
265 independent transport ('elevator') domains (TMS 3, 6, 7, and 8) (Fig. 2c). Two
266 pseudosymmetrical helical hairpins (HP1 and HP2) between TM6 and TM8 shield the binding
267 site (Fig. 2b,c), although only HP2 was shown to be a gate both in inward and outward
268 conformations of ASCT2 [72], [73]. The quality of the density was sufficient to build a model
269 for the most of the protein, except for the flexible loops connecting transport domains to the
270 scaffold domains (3-4 loop between TMS3 and 4) and N- and C-termini (residues 1-37 and
271 482-532 respectively), which are predicted to be disordered (Supplementary Fig. 3). The
272 transport domains are parked in the inward orientation and are detached from the scaffold in a
273 similar fashion as observed in ASCT2 [14] (rmsd \sim 2 Å). ASCT1 also possesses a docking
274 platform for the envelope proteins of retroviral origin, which protrudes in the extracellular
275 space and is formed by a long (\sim 35 amino acid) loop between segments of TM4 (Fig. 2a, e),
276 which folds into an antiparallel β -strand. This antenna-like stem is only partially conserved
277 (Fig. 2e) and is longer than in ASCT2 with an additional insert of five amino acids, namely

278 Asn-Ser-Ser-Ser-Gly. Asn201 of this insertion as well as Asn206 just right after the insert are
279 known to be glycosylated, which possibly is exploited by envelope proteins as the recognition
280 pattern.

281 The substrate binding site of ASCT1 is nearly identical to the one in ASCT2 (Fig. 2b, **d**), albeit
282 with one important substitution of C467 (ASCT2 numbering) to T459 (ASCT1 numbering).
283 This is a key residue for the substrate selectivity; in EAATs it is invariantly an arginine residue,
284 which allows binding of acidic substrates such as aspartate and glutamate [70]. In both ASCT1
285 and ASCT2 the binding cavity is negatively charged (Supplementary Fig. **4**), hence impeding
286 the binding of glutamate and aspartate, whereas the geometry of cavity restricts the entry of
287 positively charged lysine, arginine and histidine. Unfortunately, it was not possible to assign
288 the bound substrate due to the limited resolution, therefore the direct comparison of substrate
289 binding modes currently is not possible. Nevertheless, MD simulations indicate that the binding
290 modes are likely to be very similar (Supplementary Fig. **5**).

291 At the obtained resolution it is also impossible to assign sodium ions. However, taking
292 into account the conservation of the binding sites in the SLC1 family, positions of sodium ions
293 in archaeal homolog Glt_{Tk} [74] as well as results of MD simulations performed earlier for
294 ASCT2 [75], the most probable sodium binding residues in ASCT1 are as follows: site 1 –
295 E465, D467; site 2 – T376, V418, and site 3 – F121, T124, T125, N378, D380 respectively
296 (Fig. **2d**). **This is mostly in agreement with the recently proposed positions of sodium ions in**
297 **ASCT1 based on homology modelling** [17].

298

299 3.3. *Impact of mutations*

300 The resolution of the obtained reconstruction is sufficient to map the mutations shown to be
301 disease-related (Fig. 3). Mutation of Glu256 to Lys (E256K) is known to reduce the uptake of
302 substrates [46]. **We performed the *in vitro* characterization of this mutant, which indeed**
303 **revealed about 30-40% decrease in the uptake of radioactive L-Ser and L-Ala (Fig. 1f).**
304 **Residue 256** is located at the base of the transporter, in the first part of the TM5 scaffold helix,
305 and in the wildtype protein its side chain either interacts with the preceding Asn255 residue or
306 is fully solvent exposed. This position is relatively far from the transport domains (~ 13 Å away
307 from HP2), therefore it is hard to envision how substitution to Lys could affect the transport
308 rates. Based on the obtained structure we can propose that Lys at this position can either (i)
309 make a polar contact with Ser100 of TM2 scaffold helix which in turn interacts with TM3 of
310 the transport domain; or (ii) make a salt bridge with Glu243 of TM5 of the neighboring
311 protomer, which is in turn coordinates TM3 of the same neighboring protomer, or (iii) perhaps

312 even attract and anchor HP2 as it was seen in ASCT2 that HP2 opens towards this part of the
313 protein [73]. To check if any of these scenarios are possible, we performed all-atom MD
314 simulations that confirmed the scenario (ii) – we observed the formation of Lys256-Glu243' (**it**
315 **stands for an adjacent protomer**) salt bridge, which remained stable over 400 ns of simulation
316 time (Supplementary Figs. 6, 9-10).

317 Another well characterized mutation is R457W and it leads to the complete loss of
318 substrate uptake [46]. **We were able to reproduce this result in our experimental setup, where**
319 **the uptake of radioactive substrates was at the level of empty liposomes (Fig. 1f).** R457 of
320 TM8 of the transport domain is located nearby the substrate binding site and somewhat sits in-
321 between HP1 and HP2 elements. Judging from this location, introduction of the bulky sidechain
322 at this position might interfere with the normal function of the gate, securing the substrate site,
323 hence probably preventing substrate loading or discharge. MD simulations revealed a peculiar
324 arrangement, where W457 side chain forms a stable S- π interaction [76] with the side chain of
325 Cys343 (Supplementary Figs. 7, 9-10), hence anchoring HP1 and pulling TMS8 out of this
326 position. This is accompanied by the significant opening of HP2, which moves ~ 7 Å towards
327 the scaffold domain (Supplementary Fig. 7).

328 There is another rare mutation characterized recently, namely G381R. This residue sits
329 in the essentially conserved Asn-Met-Asp-Gly motif of TMS7, known to play an important
330 role in the formation of sodium binding sites and coupling of sodium and substrate binding
331 [74], [77]. Intriguingly, at this position the closest interaction of TMS7 and TMS8 is observed,
332 hence the replacement of Gly to Arg must have very dramatic consequences, leading to the
333 distortion of both cation and substrate binding sites, thus rendering transporter to be non-
334 functional. MD simulations revealed a significant effect of the G381R mutation on the entire
335 substrate-binding pocket, causing destabilization of the helices in the ligand-binding site and
336 rearrangement of the HP1 and HP2 loops (Supplementary Figs. 8-10). Such deformations seem
337 not to be compatible with the normal ASCT1 function [49]. **This might be also the reason why**
338 **we failed to produce this mutant.**

339

340 4. Discussion

341 In here presented structure of ASCT1 extends the number of structurally characterized
342 members of the SLC1 family, with structures available for ASCT2 [14], [72], EAAT1 [70] and
343 EAAT3 [71]. All of these reported structures are very similar in general – arranged in trimers
344 with the scaffold domains making a core with the transport domains at the periphery, which is
345 also reflected in a highly conserved transport mechanism, described as a one-gate elevator

346 movement across the membrane. Still there is a number of major differences between the two
347 subfamilies. ASCT proteins have a long insertion in-between segments of TMS4, which forms
348 a so-called docking platform made of three (one from each protomer) β -hairpins with the
349 extended loops, decorated by glycosylation. This platform can be recognized by the envelope
350 proteins of endo- or exogenous retroviruses [78], [79], which ultimately leads to the membrane
351 (and cell) fusion. In humans **such interactions** are essential during the placenta formation [80],
352 and occur between a product of Human Endogenous Retrovirus Group W family 1 member,
353 also termed syncytin-1, and ASCT1 and ASCT2 proteins, at least *in vitro* [79].

354 The other distinct feature of ASCT proteins compared to EAATs is that the former
355 perform the exchange of neutral amino acids, whereas the latter are capable to concentrate
356 acidic amino acids against the gradient. This implies that the substrate transport in EAATs is
357 unidirectional, and ASCTs perform equilibration of the amino acid pools, therefore it is quite
358 likely that ASCTs should not have any apo-states. That would also mean that the sodium-
359 substrate coupling mechanism described for EAATs and archaeal homologues, should not be
360 applicable to ASCTs. However the analysis of the differences in the ion coupling have to be
361 postponed until higher resolution structures are obtained.

362 As seen from the analysis of binding sites, the substrate specificity is dictated by the
363 charge of a cavity, which selects for negatively charged (EAATs) or neutral (ASCTs) substrates
364 and by its geometry, which excludes the access of the bulky amino acids. ASCT1 and ASCT2
365 have overlapping substrate specificities, albeit ASCT1 cannot transport glutamine [27], (Fig.
366 1), which perhaps is caused by a narrower binding site (Supplementary Fig. 4), but it can
367 accommodate (hydroxy)-proline, which is readily transported [27], [41], (Fig 1). The
368 emerging picture that despite L- and D-Ser are substrates of both ASCT1 and ASCT2, the
369 former might be the main serine transporter in the brain [39]. It must be noted though, that
370 there is no real consensus whether there is indeed preferential expression of ASCT1 in
371 astrocytes and of ASCT2 in neurons, as results are contradictory and vary with the different
372 experimental techniques [18], [81]–[84].

373 It is puzzling, that the transport in ASCT1 is negatively affected by cholesterol (Fig. 1),
374 although previously we observed the opposite effect for ASCT2, where 10% of added
375 cholesterol led to twice the amount of transported substrate [14]. In the adult brain, the majority
376 of cholesterol is synthesized in the astrocytes, which is redistributed to neurons [85], and the
377 cholesterol content in the plasma membranes of the latter is about twice less [86]. Whether
378 there is a real correlation between the cholesterol content in the membrane, localization of a

379 transporter and its kinetics remains to be explored, preferably using systems better mimicking
380 the lipid composition of human cells.

381 Mutations profiled in ASCT1 further supports the idea of its major role in the transport
382 of D-Ser and neurodevelopment. Malfunctioning of ASCT1 leads to early developmental
383 delays, spastic tetraplegia, thin corpus callosum, and progressive microcephaly [44], [46]–[48].
384 The carriers unable to develop motor skills for independent walking, typically unable to speak
385 and have severe intellectual disability. Importantly these conditions appear even if ASCT2 is
386 intact. And as seen from our functional characterization – E256K leads to the diminished
387 exchange of substrates, whereas R457W completely abolishes the transport (Fig. 1f).
388 MD simulations further corroborate that the characterized mutations might either interfere with
389 the movements of a transport domain (E256K) or disturb the loading / unloading of a substrate
390 (R457W). The third point mutation G381R is very destabilizing and leads to the collapse of the
391 binding site.

392 To summarize, our data confirm that ASCT1 is a neutral amino acid exchanger with
393 the preference for Ala, Cys, Thr, Asn, Pro and both L- and D-Ser. The obtained structure is
394 instrumental to map the point mutations in ASCT1, our functional analysis confirms the impact
395 of mutations on the transport activity and MD simulations explain how these mutations hinder
396 the transport of substrates.

397 **Author contributions:**

398 Conceptualization: AG

399 Methodology: AG, SJM, CG

400 Investigation: AS, PS, MN, NGA

401 Visualization: AS, PS, MN, NGA, SJM, CG, AG

402 Supervision: CG, SJM, AG

403 Writing—original draft: AS, AG

404 Writing—review & editing: AG

405
406 **Competing interests:** Authors declare that they have no competing interests

407
408 **Acknowledgments:**

409 We thank Dirk J. Slotboom for discussions related to this manuscript.

410
411 **Funding:**

412 Dutch Scientific Organization NWO, OCENW.KLEIN.141 (AG)

413
414
415 **Data and materials availability:** Atomic coordinates and the corresponding electron
416 microscopy density map are deposited in the Protein Data Bank and the Electron
417 Microscopy Data Bank under accession number 7P4I and EMD-13193, respectively.
418 Models and parameter files used for MD simulations are freely available from the
419 Zenodo website at the following url <https://doi.org/10.5281/zenodo.5092014>

420
421422 **References**

423

- 424 [1] Y. Kanai and M. A. Hediger, "The glutamate/neutral amino acid transporter family SLC1: Molecular,
425 physiological and pharmacological aspects," *Pflugers Arch. Eur. J. Physiol.*, vol. 447, no. 5, pp. 469–
426 479, 2004, doi: 10.1007/s00424-003-1146-4.
- 427 [2] Y. Kanai *et al.*, "The SLC1 high-affinity glutamate and neutral amino acid transporter family," *Mol.*
428 *Aspects Med.*, vol. 34, no. 2–3, pp. 108–120, 2013, doi: 10.1016/j.mam.2013.01.001.
- 429 [3] C. Grewer, A. Gameiro, and T. Rauen, "SLC1 glutamate transporters," *Pflugers Arch. Eur. J. Physiol.*,
430 vol. 466, no. 1, pp. 3–24, 2014, doi: 10.1007/s00424-013-1397-7.
- 431 [4] B. I. Kanner and I. Sharon, "Active Transport of L-Glutamate by Membrane Vesicles Isolated from Rat
432 Brain," *Biochemistry*, vol. 17, no. 19, pp. 3949–3953, 1978, doi: 10.1021/bi00612a011.
- 433 [5] N. Zerangue and M. P. Kavanaugh, "Flux coupling in a neuronal glutamate transporter," *Nature*, vol.
434 383, no. 6601, pp. 634–637, 1996, doi: 10.1038/383634a0.
- 435 [6] J. Rothstein *et al.*, "Antisense knockout of glutamate transporters reveals a predominant role for
436 astroglial glutamate transport in excitotoxicity and clearance of extracellular glutamate," *Neuron*, vol.
437 16, pp. 675–686, 1996, [Online]. Available: papers2://publication/uuid/327F682D-2D03-48C7-A0E6-
438 A57E2CD92157.
- 439 [7] Y. Zhang, A. Bendahan, R. Zarbiv, M. P. Kavanaugh, and B. I. Kanner, "Molecular determinant of ion
440 selectivity of a (Na⁺ + K⁺)-coupled rat brain glutamate transporter," *Proc. Natl. Acad. Sci. U. S. A.*, vol.
441 95, no. 2, pp. 751–755, 1998, doi: 10.1073/pnas.95.2.751.
- 442 [8] G. Pines and B. I. Kanner, "Counterflow of L-Glutamate in Plasma Membrane Vesicles and
443 Reconstituted Preparations from Rat Brain," *Biochemistry*, vol. 29, no. 51, pp. 11209–11214, 1990, doi:
444 10.1021/bi00503a008.
- 445 [9] J. L. Arriza, S. Eliasof, M. P. Kavanaugh, and S. G. Amara, "Excitatory amino acid transporter 5, a
446 retinal glutamate transporter coupled to a chloride conductance," *Proc. Natl. Acad. Sci. U. S. A.*, vol. 94,
447 no. 8, pp. 4155–4160, 1997, doi: 10.1073/pnas.94.8.4155.
- 448 [10] N. Utsunomiya-Tate, H. Endou, and Y. Kanai, "Cloning and functional characterization of a system
449 ASC-like Na⁺-dependent neutral amino acid transporter," *J. Biol. Chem.*, vol. 271, no. 25, pp. 14883–
450 14890, 1996, doi: 10.1074/jbc.271.25.14883.
- 451 [11] G. P. Leary, E. F. Stone, D. C. Holley, and M. P. Kavanaugh, "The glutamate and chloride permeation
452 pathways are colocalized in individual neuronal glutamate transporter subunits," *J. Neurosci.*, vol. 27,
453 no. 11, pp. 2938–2942, 2007, doi: 10.1523/JNEUROSCI.4851-06.2007.
- 454 [12] J. I. Wadiche, S. G. Amara, and M. P. Kavanaugh, "Ion fluxes associated with excitatory amino acid
455 transport," *Neuron*, vol. 15, no. 3, pp. 721–728, 1995, doi: 10.1016/0896-6273(95)90159-0.
- 456 [13] B. Billups, D. Rossi, and D. Attwell, "Anion conductance behavior of the glutamate uptake carrier in
457 salamander retinal glial cells," *J. Neurosci.*, vol. 16, no. 21, pp. 6722–6731, 1996, doi:
458 10.1523/jneurosci.16-21-06722.1996.
- 459 [14] A. A. Garaeva, G. T. Oostergetel, C. Gati, A. Guskov, C. Paulino, and D. J. Slotboom, "Cryo-EM
460 structure of the human neutral amino acid transporter ASCT2," *Nat. Struct. Mol. Biol.*, vol. 25, no. 6,
461 pp. 515–521, 2018, doi: 10.1038/s41594-018-0076-y.
- 462 [15] A. Bröer, C. Wagner, F. Lang, and S. Bröer, "Neutral amino acid transporter ASCT2 displays substrate-
463 induced Na⁺ exchange and a substrate-gated anion conductance," *Biochem. J.*, vol. 346, no. 3, pp. 705–
464 710, 2000, doi: 10.1042/0264-6021:3460705.

- 465 [16] N. Zerangue and M. P. Kavanaugh, "ASCT-1 is a neutral amino acid exchanger with chloride channel
466 activity," *J. Biol. Chem.*, vol. 271, no. 45, pp. 27991–27994, 1996, doi: 10.1074/jbc.271.45.27991.
- 467 [17] M. Scalise, L. Console, J. Cosco, L. Pochini, M. Galluccio, and C. Indiveri, "ASCT1 and ASCT2:
468 Brother and Sister?," *SLAS Discov.*, 2021, doi: 10.1177/24725552211030288.
- 469 [18] K. Sakai, H. Shimizu, T. Koike, S. Furuya, and M. Watanabe, "Neutral amino acid transporter ASCT1
470 is preferentially expressed in L-Ser-synthetic/storing glial cells in the mouse brain with transient
471 expression in developing capillaries," *J. Neurosci.*, vol. 23, no. 2, pp. 550–560, 2003, doi:
472 10.1523/jneurosci.23-02-00550.2003.
- 473 [19] J. L. Arriza *et al.*, "Cloning and expression of a human neutral amino acid transporter with structural
474 similarity to the glutamate transporter gene family," *J. Biol. Chem.*, vol. 268, no. 21, pp. 15329–15332,
475 1993, doi: 10.1016/s0021-9258(18)82257-8.
- 476 [20] S. Shafgat *et al.*, "Cloning and expression of a novel Na⁺-dependent neutral amino acid transporter
477 structurally related to mammalian Na⁺/glutamate cotransporters," *J. Biol. Chem.*, vol. 268, no. 21, pp.
478 15351–15355, 1993, doi: 10.1016/s0021-9258(18)82263-3.
- 479 [21] M. A. Hediger, B. Cl  men  on, R. E. Burrier, and E. A. Bruford, "The ABCs of membrane transporters
480 in health and disease (SLC series): Introduction," *Mol. Aspects Med.*, vol. 34, no. 2–3, pp. 95–107,
481 2013, doi: 10.1016/j.mam.2012.12.009.
- 482 [22] H. Jiang, N. Zhang, T. Tang, F. Feng, H. Sun, and W. Qu, "Target the human Alanine/Serine/Cysteine
483 Transporter 2(ASCT2): Achievement and Future for Novel Cancer Therapy," *Pharmacol. Res.*, vol.
484 158, no. May, p. 104844, 2020, doi: 10.1016/j.phrs.2020.104844.
- 485 [23] M. Scalise, L. Pochini, M. Galluccio, L. Console, and C. Indiveri, "Glutamine transport and
486 mitochondrial metabolism in cancer cell growth," *Front. Oncol.*, vol. 7, no. DEC, pp. 1–9, 2017, doi:
487 10.3389/fonc.2017.00306.
- 488 [24] R. J. DeBerardinis *et al.*, "Beyond aerobic glycolysis: Transformed cells can engage in glutamine
489 metabolism that exceeds the requirement for protein and nucleotide synthesis," *Proc. Natl. Acad. Sci. U.
490 S. A.*, vol. 104, no. 49, pp. 19345–19350, 2007, doi: 10.1073/pnas.0709747104.
- 491 [25] M. Younes, M. Pathak, D. Finnie, R. N. Sifers, Y. Liu, and M. R. Schwartz, "Expression of the neutral
492 amino acids transporter ASCT1 in esophageal carcinomas," *Anticancer Res.*, vol. 20, no. 5C, pp. 3775–
493 3779, Sep. 2000.
- 494 [26] Q. Wang *et al.*, "Targeting amino acid transport in metastatic castration-resistant prostate cancer: Effects
495 on cell cycle, cell growth, and tumor development," *J. Natl. Cancer Inst.*, vol. 105, no. 19, pp. 1463–
496 1473, 2013, doi: 10.1093/jnci/djt241.
- 497 [27] J. Pinilla-Tenas, A. Barber, and M. P. Lostao, "Transport of proline and hydroxyproline by the neutral
498 amino-acid exchanger ASCT1," *J. Membr. Biol.*, vol. 195, no. 1, pp. 27–32, 2003, doi: 10.1007/s00232-
499 003-2041-9.
- 500 [28] J. H. Yang *et al.*, "Brain-specific Phgdh deletion reveals a pivotal role for l-serine biosynthesis in
501 controlling the level of D-serine, an N-methyl-D-aspartate receptor co-agonist, in adult brain," *J. Biol.
502 Chem.*, vol. 285, no. 53, pp. 41380–41390, 2010, doi: 10.1074/jbc.M110.187443.
- 503 [29] M. J. Schell, M. E. Molliver, and S. H. Snyder, "D-serine, an endogenous synaptic modulator:
504 Localization to astrocytes and glutamate-stimulated release," *Proc. Natl. Acad. Sci. U. S. A.*, vol. 92, no.
505 9, pp. 3948–3952, 1995, doi: 10.1073/pnas.92.9.3948.
- 506 [30] I. Radziszewsky, H. Sason, and H. Wolosker, "D-Serine: Physiology and pathology," *Curr. Opin. Clin.
507 Nutr. Metab. Care*, vol. 16, no. 1, pp. 72–75, 2013, doi: 10.1097/MCO.0b013e32835a3466.
- 508 [31] A. Hashimoto, T. Nishikawa, T. Oka, and K. Takahashi, "Endogenous d-Serine in Rat Brain:
509 N-Methyl-d-Aspartate Receptor-Related Distribution and Aging," *J. Neurochem.*, vol. 60, no. 2, pp.

- 510 783–786, 1993, doi: 10.1111/j.1471-4159.1993.tb03219.x.
- 511 [32] J. P. Mothet *et al.*, “D-serine is an endogenous ligand for the glycine site of the N-methyl-D-aspartate
512 receptor,” *Proc. Natl. Acad. Sci. U. S. A.*, vol. 97, no. 9, pp. 4926–4931, 2000, doi:
513 10.1073/pnas.97.9.4926.
- 514 [33] H. Wolosker, S. Blackshaw, and S. H. Snyder, “Serine racemase: A glial enzyme synthesizing D-serine
515 to regulate glutamate-N-methyl-D-aspartate neurotransmission,” *Proc. Natl. Acad. Sci. U. S. A.*, vol. 96,
516 no. 23, pp. 13409–13414, 1999, doi: 10.1073/pnas.96.23.13409.
- 517 [34] K. Miya *et al.*, “Serine racemase is predominantly localized in neurons in mouse brain,” *J. Comp.*
518 *Neurol.*, vol. 510, no. 6, pp. 641–654, 2008, doi: 10.1002/cne.21822.
- 519 [35] J. T. Ehmsen *et al.*, “D-serine in glia and neurons derives from 3-phosphoglycerate dehydrogenase,” *J.*
520 *Neurosci.*, vol. 33, no. 30, pp. 12464–12469, 2013, doi: 10.1523/JNEUROSCI.4914-12.2013.
- 521 [36] M. A. Benneyworth, Y. Li, A. C. Basu, V. Y. Bolshakov, and J. T. Coyle, “Cell selective conditional
522 null mutations of serine racemase demonstrate a predominate localization in cortical glutamatergic
523 neurons,” *Cell. Mol. Neurobiol.*, vol. 32, no. 4, pp. 613–624, 2012, doi: 10.1007/s10571-012-9808-4.
- 524 [37] M. Yamasaki, K. Yamada, S. Furuya, J. Mitoma, Y. Hirabayashi, and M. Watanabe, “3-
525 Phosphoglycerate dehydrogenase, a key enzyme for L-serine biosynthesis, is preferentially expressed in
526 the radial glia/astrocyte lineage and olfactory ensheathing glia in the mouse brain,” *J. Neurosci.*, vol. 21,
527 no. 19, pp. 7691–7704, 2001, doi: 10.1523/jneurosci.21-19-07691.2001.
- 528 [38] H. Wolosker, “Serine racemase and the serine shuttle between neurons and astrocytes,” *Biochim.*
529 *Biophys. Acta - Proteins Proteomics*, vol. 1814, no. 11, pp. 1558–1566, 2011, doi:
530 10.1016/j.bbapap.2011.01.001.
- 531 [39] E. Kaplan *et al.*, “ASCT1 (Slc1a4) transporter is a physiologic regulator of brain D-serine and
532 neurodevelopment,” *Proc. Natl. Acad. Sci. U. S. A.*, vol. 115, no. 38, pp. 9628–9633, 2018, doi:
533 10.1073/pnas.1722677115.
- 534 [40] Y. Kasai, M. Tachikawa, S. Hirose, S. I. Akanuma, and K. I. Hosoya, “Transport systems of serine at
535 the brain barriers and in brain parenchymal cells,” *J. Neurochem.*, vol. 118, no. 2, pp. 304–313, 2011,
536 doi: 10.1111/j.1471-4159.2011.07313.x.
- 537 [41] A. C. Foster *et al.*, “D-serine is a substrate for neutral amino acid transporters ASCT1/SLC1A4 and
538 ASCT2/SLC1A5, and is transported by both subtypes in rat hippocampal astrocyte cultures,” *PLoS One*,
539 vol. 11, no. 6, pp. 1–18, 2016, doi: 10.1371/journal.pone.0156551.
- 540 [42] C. M. Gliddon, Z. Shao, J. L. LeMaistre, and C. M. Anderson, “Cellular distribution of the neutral
541 amino acid transporter subtype ASCT2 in mouse brain,” *J. Neurochem.*, vol. 108, no. 2, pp. 372–383,
542 2009, doi: 10.1111/j.1471-4159.2008.05767.x.
- 543 [43] S. Bhat, A. El-Kasaby, M. Freissmuth, and S. Sucic, “Functional and Biochemical Consequences of
544 Disease Variants in Neurotransmitter Transporters: A Special Emphasis on Folding and Trafficking
545 Deficits,” *Pharmacol. Ther.*, vol. 222, p. 107785, 2021, doi: 10.1016/j.pharmthera.2020.107785.
- 546 [44] H. A. Abdelrahman, A. Al-Shamsi, A. John, B. R. Ali, and L. Al-Gazali, “A Novel SLC1A4 Mutation
547 (p.Y191*) Causes Spastic Tetraplegia, Thin Corpus Callosum, and Progressive Microcephaly
548 (SPATCCM) With Seizure Disorder,” *Child Neurol. Open*, vol. 6, p. 2329048X1988064, 2019, doi:
549 10.1177/2329048x19880647.
- 550 [45] J. Conroy *et al.*, “Novel European SLC1A4 variant: Infantile spasms and population ancestry analysis,”
551 *J. Hum. Genet.*, vol. 61, no. 8, pp. 761–764, 2016, doi: 10.1038/jhg.2016.44.
- 552 [46] N. Damseh *et al.*, “Mutations in SLC1A4, encoding the brain serine transporter, are associated with
553 developmental delay, microcephaly and hypomyelination,” *J. Med. Genet.*, vol. 52, no. 8, pp. 541–547,
554 2015, doi: 10.1136/jmedgenet-2015-103104.

- 555 [47] G. Heimer *et al.*, “SLC1A4 mutations cause a novel disorder of intellectual disability, progressive
556 microcephaly, spasticity and thin corpus callosum,” *Clin. Genet.*, vol. 88, no. 4, pp. 327–335, 2015, doi:
557 10.1111/cge.12637.
- 558 [48] M. Srour *et al.*, “A homozygous mutation in SLC1A4 in siblings with severe intellectual disability and
559 microcephaly,” *Clin. Genet.*, vol. 88, no. 1, pp. E1–E4, Jul. 2015, doi: 10.1111/cge.12605.
- 560 [49] E. Pironti *et al.*, “A novel SLC1A4 homozygous mutation causing congenital microcephaly, epileptic
561 encephalopathy and spastic tetraparesis: a video-EEG and tractography–case study,” *J. Neurogenet.*, vol.
562 32, no. 4, pp. 316–321, 2018, doi: 10.1080/01677063.2018.1476510.
- 563 [50] M. Schorb, I. Haberbosch, W. J. H. Hagen, Y. Schwab, and D. N. Mastronarde, “Software tools for
564 automated transmission electron microscopy,” *Nat. Methods*, vol. 16, no. 6, pp. 471–477, 2019, doi:
565 10.1038/s41592-019-0396-9.
- 566 [51] S. H. W. Scheres, “RELION: Implementation of a Bayesian approach to cryo-EM structure
567 determination,” *J. Struct. Biol.*, vol. 180, no. 3, pp. 519–530, 2012, doi: 10.1016/j.jsb.2012.09.006.
- 568 [52] S. Q. Zheng, E. Palovcak, J. P. Armache, K. A. Verba, Y. Cheng, and D. A. Agard, “MotionCor2:
569 Anisotropic correction of beam-induced motion for improved cryo-electron microscopy,” *Nat. Methods*,
570 vol. 14, no. 4, pp. 331–332, 2017, doi: 10.1038/nmeth.4193.
- 571 [53] A. Rohou and N. Grigorieff, “CTFFIND4: Fast and accurate defocus estimation from electron
572 micrographs,” *J. Struct. Biol.*, vol. 192, no. 2, pp. 216–221, 2015, doi: 10.1016/j.jsb.2015.08.008.
- 573 [54] A. Punjani, H. Zhang, and D. J. Fleet, “Non-uniform refinement: adaptive regularization improves
574 single-particle cryo-EM reconstruction,” *Nat. Methods*, vol. 17, no. 12, pp. 1214–1221, 2020, doi:
575 10.1038/s41592-020-00990-8.
- 576 [55] M. J. Abraham *et al.*, “Gromacs: High performance molecular simulations through multi-level
577 parallelism from laptops to supercomputers,” *SoftwareX*, vol. 1–2, pp. 19–25, 2015, doi:
578 10.1016/j.softx.2015.06.001.
- 579 [56] J. Huang and A. D. Mackerell, “CHARMM36 all-atom additive protein force field: Validation based on
580 comparison to NMR data,” *J. Comput. Chem.*, vol. 34, no. 25, pp. 2135–2145, 2013, doi:
581 10.1002/jcc.23354.
- 582 [57] J. B. Klauda *et al.*, “Update of the CHARMM All-Atom Additive Force Field for Lipids: Validation on
583 Six Lipid Types,” *J. Phys. Chem. B*, vol. 114, no. 23, pp. 7830–7843, 2010, doi: 10.1021/jp101759q.
- 584 [58] E. L. Wu *et al.*, “CHARMM-GUI membrane builder toward realistic biological membrane simulations,”
585 *J. Comput. Chem.*, vol. 35, no. 27, pp. 1997–2004, 2014, doi: 10.1002/jcc.23702.
- 586 [59] J. Lee *et al.*, “CHARMM-GUI Input Generator for NAMD, GROMACS, AMBER, OpenMM, and
587 CHARMM/OpenMM Simulations Using the CHARMM36 Additive Force Field,” *J. Chem. Theory
588 Comput.*, vol. 12, no. 1, pp. 405–413, 2016, doi: 10.1021/acs.jctc.5b00935.
- 589 [60] S. Jo, T. Kim, V. G. Iyer, and W. Im, “CHARMM-GUI: A web-based graphical user interface for
590 CHARMM,” *J. Comput. Chem.*, vol. 29, no. 11, pp. 1859–1865, Aug. 2008, doi: 10.1002/jcc.20945.
- 591 [61] W. L. Jorgensen, J. Chandrasekhar, J. D. Madura, R. W. Impey, and M. L. Klein, “Comparison of
592 simple potential functions for simulating liquid water,” *J. Chem. Phys.*, vol. 79, no. 2, pp. 926–935,
593 1983, doi: 10.1063/1.445869.
- 594 [62] U. Essmann, L. Perera, M. L. Berkowitz, T. Darden, H. Lee, and L. G. Pedersen, “A smooth particle
595 mesh Ewald method,” *J. Chem. Phys.*, vol. 103, no. 19, pp. 8577–8593, 1995, doi: 10.1063/1.470117.
- 596 [63] T. Darden, D. York, and L. Pedersen, “Particle mesh Ewald: An $N \cdot \log(N)$ method for Ewald sums in
597 large systems,” *J. Chem. Phys.*, vol. 98, no. 12, pp. 10089–10092, 1993, doi: 10.1063/1.464397.

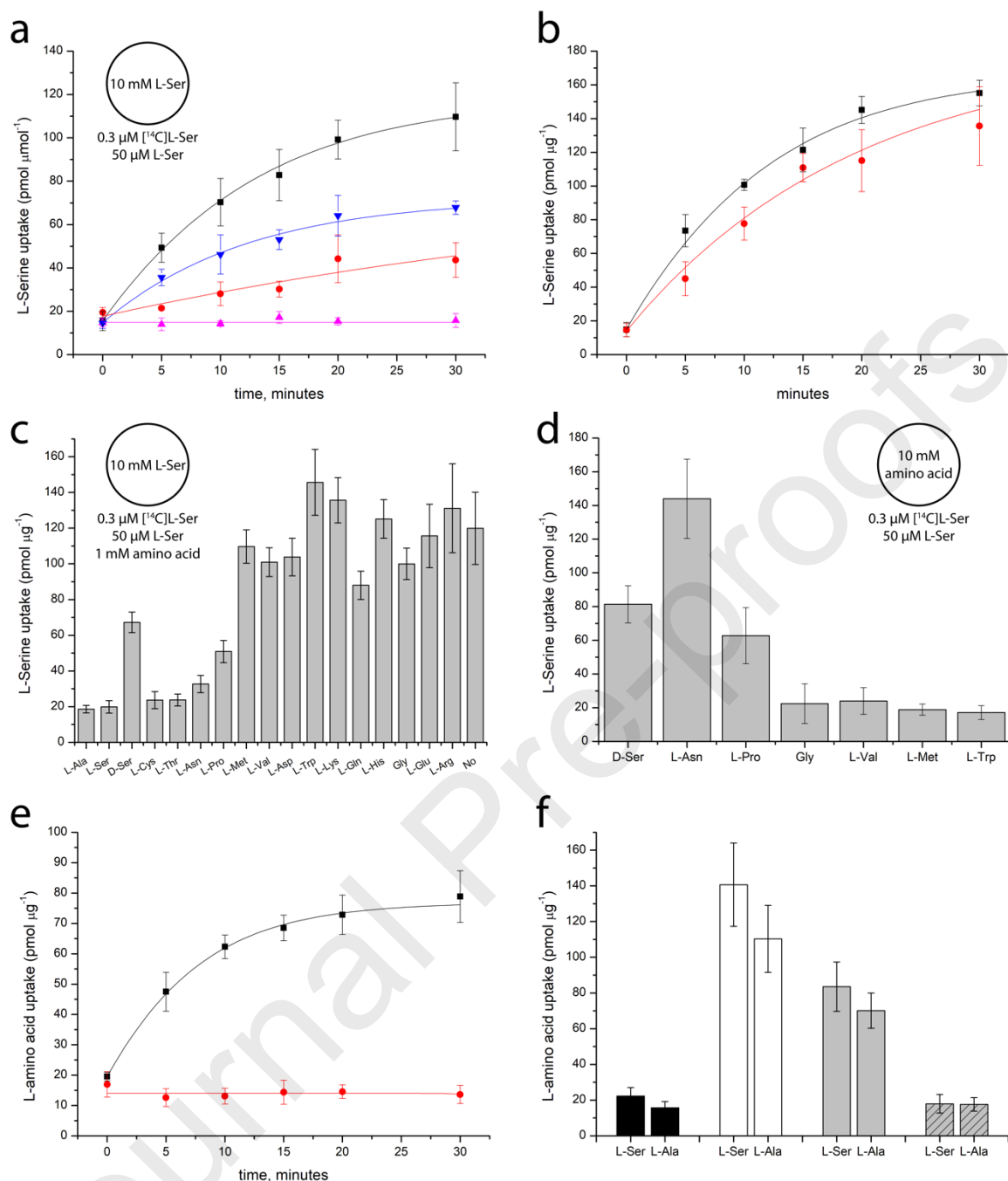
- 598 [64] M. Parrinello and A. Rahman, "Polymorphic transitions in single crystals: A new molecular dynamics
599 method," *J. Appl. Phys.*, vol. 52, no. 12, pp. 7182–7190, 1981, doi: 10.1063/1.328693.
- 600 [65] S. Nosé and M. L. Klein, "Constant pressure molecular dynamics for molecular systems," *Mol. Phys.*,
601 vol. 50, no. 5, pp. 1055–1076, 1983, doi: 10.1080/00268978300102851.
- 602 [66] S. Nosé, "A unified formulation of the constant temperature molecular dynamics methods," *J. Chem.*
603 *Phys.*, vol. 81, no. 1, pp. 511–519, 1984, doi: 10.1063/1.447334.
- 604 [67] W. G. Hoover, "Canonical dynamics: Equilibrium phase-space distributions," *Phys. Rev. A*, vol. 31, no.
605 3, pp. 1695–1697, Mar. 1985, doi: 10.1103/PhysRevA.31.1695.
- 606 [68] W. Humphrey, A. Dalke, and K. Schulten, "VMD: Visual molecular dynamics," *J. Mol. Graph.*, vol. 14,
607 no. 1, pp. 33–38, Feb. 1996, doi: 10.1016/0263-7855(96)00018-5.
- 608 [69] E. R. Geertsma, N. A. B. Nik Mahmood, G. K. Schuurman-Wolters, and B. Poolman, "Membrane
609 reconstitution of ABC transporters and assays of translocator function," *Nat. Protoc.*, vol. 3, no. 2, pp.
610 256–266, 2008, doi: 10.1038/nprot.2007.519.
- 611 [70] J. C. Canul-Tec *et al.*, "Structure and allosteric inhibition of excitatory amino acid transporter 1,"
612 *Nature*, vol. 544, no. 7651, pp. 446–451, 2017, doi: 10.1038/nature22064.
- 613 [71] B. Qiu, D. Matthies, E. Fortea, Z. Yu, and O. Boudker, "Cryo-EM structures of excitatory amino acid
614 transporter 3 visualize coupled substrate, sodium, and proton binding and transport," *Sci. Adv.*, vol. 7,
615 no. 10, pp. 1–10, 2021, doi: 10.1126/sciadv.abf5814.
- 616 [72] X. Yu *et al.*, "Cryo-EM structures of the human glutamine transporter SLC1a5 (ASCT2) in the outward-
617 facing conformation," *Elife*, vol. 8, pp. 1–17, 2019, doi: 10.7554/eLife.48120.
- 618 [73] A. A. Garaeva, A. Guskov, D. J. Slotboom, and C. Paulino, "A one-gate elevator mechanism for the
619 human neutral amino acid transporter ASCT2," *Nat. Commun.*, vol. 10, no. 1, pp. 1–8, 2019, doi:
620 10.1038/s41467-019-11363-x.
- 621 [74] A. Guskov, S. Jensen, I. Faustino, S. J. Marrink, and D. J. Slotboom, "Coupled binding mechanism of
622 three sodium ions and aspartate in the glutamate transporter homologue Glt Tk," *Nat. Commun.*, vol. 7,
623 pp. 1–6, 2016, doi: 10.1038/ncomms13420.
- 624 [75] C. B. Zander, T. Albers, and C. Grewer, "Voltage-dependent processes in the electroneutral amino acid
625 exchanger ASCT2," *J. Gen. Physiol.*, vol. 141, no. 6, pp. 659–672, 2013, doi: 10.1085/jgp.201210948.
- 626 [76] A. L. Ringer, A. Senenko, and C. D. Sherrill, "Models of S/π interactions in protein structures:
627 Comparison of the H 2 S-benzene complex with PDB data," *Protein Sci.*, vol. 16, no. 10, pp. 2216–
628 2223, 2007, doi: 10.1110/ps.073002307.
- 629 [77] S. Jensen, A. Guskov, S. Rempel, I. Hänelt, and D. J. Slotboom, "Crystal structure of a substrate-free
630 aspartate transporter," *Nat. Struct. Mol. Biol.*, vol. 20, no. 10, pp. 1224–1227, 2013, doi:
631 10.1038/nsmb.2663.
- 632 [78] S. Shimode, R. Nakaoka, H. Shogen, and T. Miyazawa, "Characterization of feline ASCT1 and ASCT2
633 as RD-114 virus receptor," *J. Gen. Virol.*, vol. 94, no. PART7, pp. 1608–1612, 2013, doi:
634 10.1099/vir.0.052928-0.
- 635 [79] D. Lavillette, M. Marin, A. Ruggieri, F. Mallet, F.-L. Cosset, and D. Kabat, "The Envelope
636 Glycoprotein of Human Endogenous Retrovirus Type W Uses a Divergent Family of Amino Acid
637 Transporters/Cell Surface Receptors," *J. Virol.*, vol. 76, no. 13, pp. 6442–6452, 2002, doi:
638 10.1128/jvi.76.13.6442-6452.2002.
- 639 [80] R. M. Roberts *et al.*, "Syncytins expressed in human placental trophoblast," *Placenta*, Jan. 2021, doi:
640 10.1016/j.placenta.2021.01.006.

- 641 [81] M. D. Weiss, S. Derazi, M. S. Kilberg, and K. J. Anderson, "Ontogeny and localization of the neutral
642 amino acid transporter ASCT1 in rat brain," *Dev. Brain Res.*, vol. 130, no. 2, pp. 183–190, 2001, doi:
643 10.1016/S0165-3806(01)00250-4.
- 644 [82] A. Bröer *et al.*, "The astroglial ASCT2 amino acid transporter as a mediator of glutamine efflux," *J.*
645 *Neurochem.*, vol. 73, no. 5, pp. 2184–2194, 1999, doi: 10.1046/j.1471-4159.1999.02184.x.
- 646 [83] M. Dolińska, B. Zabłocka, U. Sonnewald, and J. Albrecht, "Glutamine uptake and expression of
647 mRNA's of glutamine transporting proteins in mouse cerebellar and cerebral cortical astrocytes and
648 neurons," *Neurochem. Int.*, vol. 44, no. 2, pp. 75–81, 2004, doi: 10.1016/S0197-0186(03)00123-2.
- 649 [84] G. S. Jeon, D. H. Choi, H. N. Lee, D. W. Kim, C. K. Chung, and S. S. Cho, "Expression of l-Serine
650 Biosynthetic Enzyme 3-Phosphoglycerate Dehydrogenase (Phgdh) and Neutral Amino Acid Transporter
651 ASCT1 Following an Excitotoxic Lesion in the Mouse Hippocampus," *Neurochem. Res.*, vol. 34, no. 5,
652 pp. 827–834, 2009, doi: 10.1007/s11064-008-9831-5.
- 653 [85] F. W. Pfrieger and N. Ungerer, "Cholesterol metabolism in neurons and astrocytes," *Prog. Lipid Res.*,
654 vol. 50, no. 4, pp. 357–371, 2011, doi: 10.1016/j.plipres.2011.06.002.
- 655 [86] A. Y. Abramov, M. Ionov, E. Pavlov, and M. R. Duchon, "Membrane cholesterol content plays a key
656 role in the neurotoxicity of β -amyloid: Implications for Alzheimer's disease," *Ageing Cell*, vol. 10, no. 4,
657 pp. 595–603, 2011, doi: 10.1111/j.1474-9726.2011.00685.x.

658

659

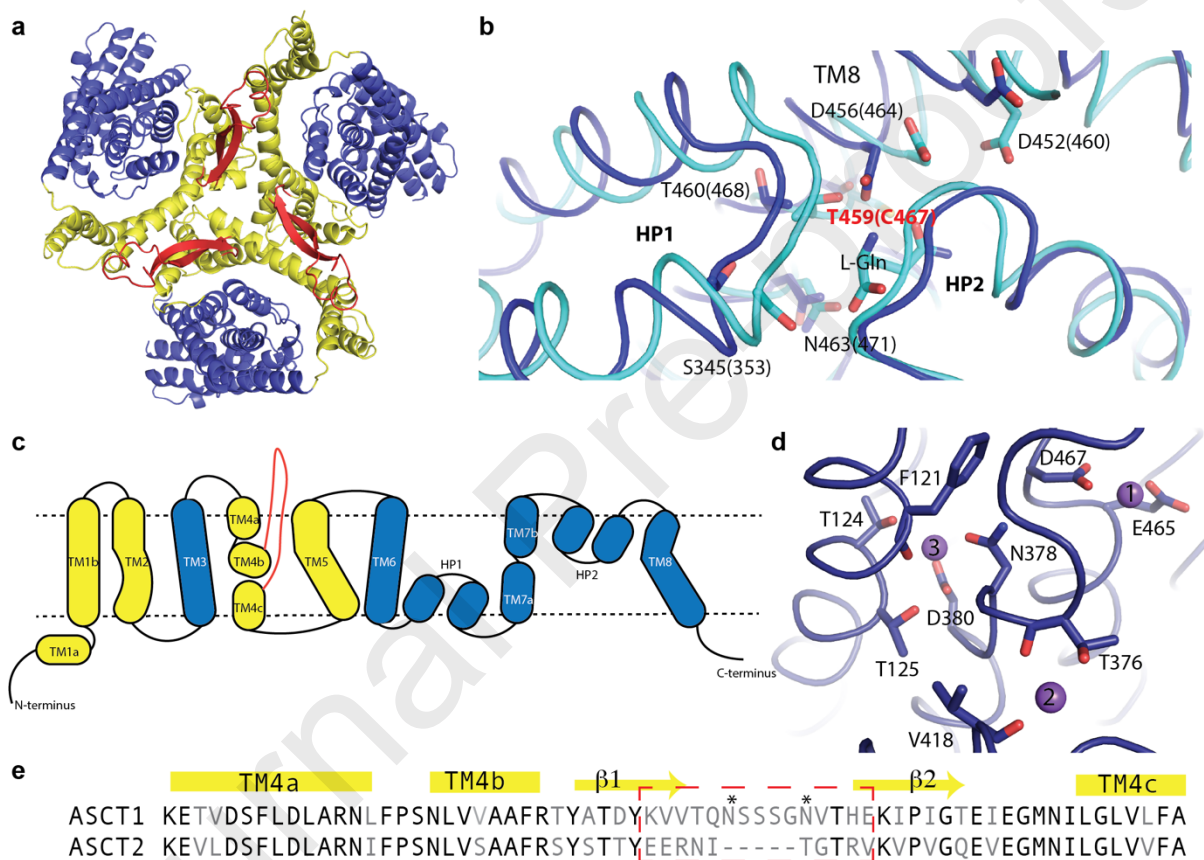
660 **Figures and Tables**

661
662

663 **Fig. 1. Functional characterization of ASCT1** (a) Exchange of internal unlabeled L-serine with
 664 external [^{14}C]L-serine in proteoliposomes with different amounts of cholesterol. Black squares -
 665 proteoliposomes without added cholesterol; blue downward triangles - with 5% (wt/wt) cholesterol; red
 666 circles - with 10% (wt/wt) cholesterol, pink triangles – **empty (no substrate inside) proteoliposomes**.
 667 (b) Electroneutral nature of exchange and sodium dependency. Black squares - 3 μM valinomycin was
 668 added at the start to proteoliposomes, loaded with 50 mM KCl; red circles - 3 μM valinomycin was
 669 added at 14 min to proteoliposomes, loaded with 50 mM KCl. (c) **Impact of a second unlabeled amino**
 670 **acid in excess, indicated in x-axis on [^{14}C]L-serine uptake.** (d) Exchange of internal unlabeled amino
 671 acid, indicated in x-axis, with external [^{14}C]L-serine in proteoliposomes. (e) Exchange of external

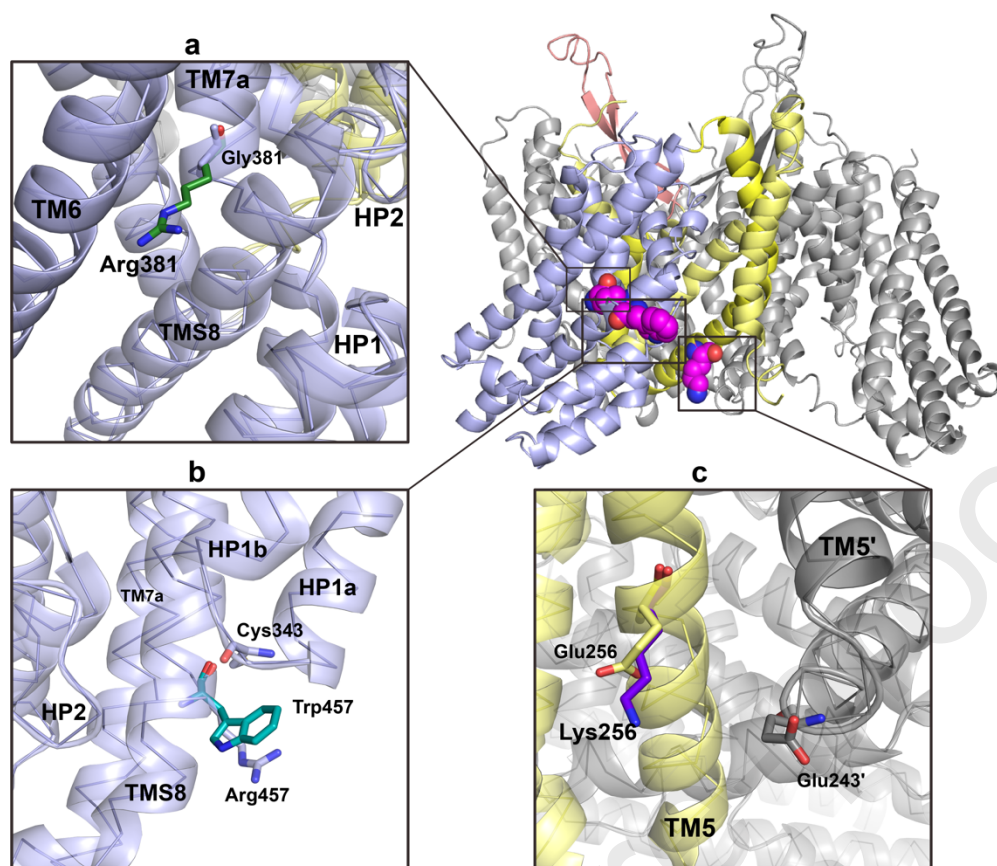
672 radioactive amino acid in proteoliposomes. Black – exchange of internal unlabeled L-alanine with
 673 external [^{14}C]L-alanine; red – exchange of internal unlabeled L-glutamine with external [^3H]L-
 674 glutamine. (f) Diminished uptake of radioactive L-serine and L-alanine – bars in black, white, gray, and
 675 slant gray for empty liposomes, WT, E256K and R457W mutants respectively. Data points and error
 676 bars represent means \pm s.e.m. from three independent experiments, each done in at least two technical
 677 replicates.

678
 679
 680



681
 682 **Fig.2 Structure of ASCT1** (a) Top view onto ASCT1 trimer (shown as cartoon). Scaffold and transport
 683 domains in yellow and blue respectively, extracellular extensions in red. (b) Superposition of binding
 684 sites between ASCT1 (blue) and ASCT2 (cyan). The main residues involved are shown as sticks and
 685 numbered (in parentheses numbering for ASCT2). The only substitution is indicated with red. (c) The
 686 secondary structure diagram, coloring as in panel a. (d) Predicted positions of sodium (purple spheres)
 687 in ASCT1. (e) The sequence alignment around the extracellular extension region. Non-identical amino
 688 acids indicated with grey. The highly variable part is within the red dashed rectangle. N-glycosylated
 689 residues marked with an *.

690
 691
 692



693

694 **Fig. 3 Disease-linked mutations in ASCT1 (a) G381R (b) R457W (c) E256K.** The scaffold and
695 transport domains in pale yellow and pale blue respectively. Upper right panel shows global positions
696 of affected residues, shown with magenta spheres. See also Supplementary Figures 6-10.

697

698

699

700

Table 1. Cryo-EM data collection, refinement and validation statistics**Data collection and processing**

Magnification	29,000
Voltage (kV)	300
Electron exposure (e ⁻ /Å ²)	60
Defocus range (μm)	-1.0 – -2.0
Pixel size (Å)	0.8521
Symmetry imposed	C3
Initial particle images (no.)	1,336,001
Final particle images (no.)	134,344
Map resolution (Å) FSC=0.143	4.2

Refinement

Initial model	PDB 6GCT
Model composition	
Nonhydrogen atoms	9510
Protein residues	1284
R.m.s. deviations	
Bond lengths (Å)	0.003
Bond angles (°)	0.69
Validation	
MolProbity score	1.96
Clashscore	11.6
Poor rotamers (%)	0.0
Ramachandran plot	
Favored (%)	94.34
Allowed (%)	5.66
Disallowed (%)	0.00
CC_mask	0.84
CC_volume	0.83

701

702

703

Author statement

704

Conceptualization: AG

705

Methodology: AG, SJM, CG

706

Investigation: AS, PS, MN, NGA

707

Visualization: AS, PS, MN, NGA, SJM, CG, AG

708

Supervision: CG, SJM, AG

709

Writing—original draft: AS, AG

710

Writing—review & editing: AG

711

712

713

Declaration of Competing Interest

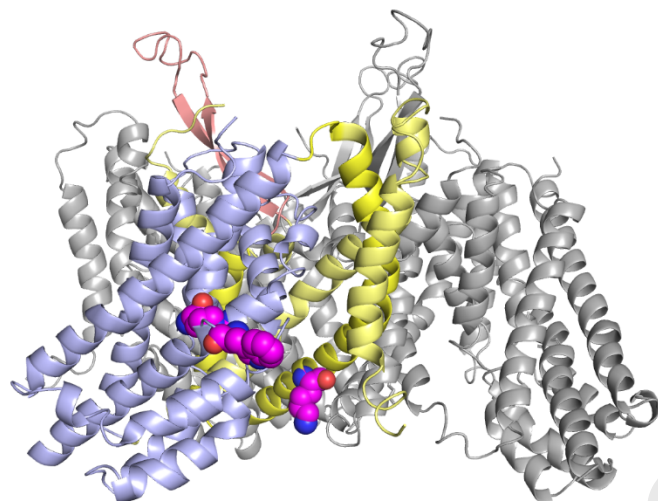
714

The authors declare that they have no known competing financial interests or personal relationships that could have appeared to influence the work reported in this paper.

715

716

717



Journal Pre-proofs